Heliyon 10 (2024) e34526

Contents lists available at ScienceDirect

Heliyon

journal homepage: www.cell.com/heliyon

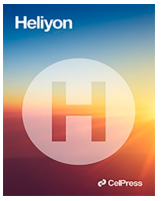

Research article

Multi-omics reveals the impact of cancer-associated fibroblasts on the prognosis and treatment response of adult diffuse highest-grade gliomas

Ganghua Zhang [1], Panpan Tai [1], Jianing Fang, Zhanwang Wang, Rui Yu, Zhijing Yin, Ke Cao [*]

Department of Oncology, Third Xiangya Hospital, Central South University, Changsha, China

ARTICLE INFO

Keywords:
Adult diffuse highest-grade gliomas
CAF
Artificial neural network
IDH mutation
Immunotherapy

ABSTRACT

Background: Cancer associated fibroblasts (CAF), an important cancer-promoting and immunosuppressive component of the tumor immune microenvironment (TIME), have recently been found to infiltrate adult diffuse highest-grade gliomas (ADHGG) (gliomas of grade IV).
Methods: Gene expression and clinical data of ADHGG patients were obtained from the CGGA and TCGA databases. Consensus clustering was used to identify CAF subtypes based on CAF key genes acquired from single-cell omics and spatial transcriptomomics. CIBERSORT, ssGSEA, MCPcounter, and ESTIMATE analyses were used to assess the TIME of GBM. Survival analysis, drug sensitivity analysis, TCIA database, TIDE and cMap algorithms were used to compare the prognosis and treatment response between patients with different CAF subtypes. An artificial neural network (ANN) model based on random forest was constructed to exactly identify CAF subtypes, which was validated in a real-world patient cohort of ADHGG.
Results: Consensus clustering classified ADHGG into two CAF subtypes. Compared with subtype B, patients with ADHGG subtype A had a poorer prognosis, worse responsiveness to immunotherapy and radiotherapy, higher CAF infiltration in TIME, but higher sensitivity to temozolomide. Furthermore, patients with subtype A had a much lower proportion of IDH mutations. Finally, the ANN model based on five genes (COL3A1, COL1A2, CD248, FN1, and COL1A1) could exactly discriminate CAF subtypes, and the validation of the real-world cohort indicated consistent results with the bioinformatics analyses.
Conclusion: This study revealed a novel CAF subtype to distinguish ADHGG patients with different prognosis and treatment responsiveness, which may be helpful for accurate clinical decision-making of ADHGG.

1. Introduction

Glioblastoma(GBM) is the most common primary tumor of the central nervous system in adults [1]. The current treatment of GBM

* Corresponding author. Department of Oncology, Third Xiangya Hospital of Central South University, 138 Tongzipo Road, Changsha, 410013, China.
E-mail address: csucaoke@163.com (K. Cao).
[1] These authors contributed equally.

https://doi.org/10.1016/j.heliyon.2024.e34526
Received 28 February 2024; Received in revised form 9 July 2024; Accepted 10 July 2024
Available online 14 July 2024

include surgery, chemotherapy and radiotherapy, but the efficacy is limited [2], with a survival time after active intervention of less than 13.5 months [3]. Potential reasons for this poor outcome include tumor evolution, high recurrence rates, incomplete resection, and resistance to radio- and chemotherapy [4,5]. Due to the obstruction of the blood-brain barrier, there is a lack of effective chemotherapy drugs in GBM patients beyond temozolomide. However, the resistance of temozolomide is common [6,7]. In addition to the limitation of treatment strategies, an optimization of the molecular classification of GBM also needs to be developed [8]. The most important markers related to the treatment of GBM are IDH mutations, 1p19q co-deletion and MGMT promoter methylation. Based on the combination of these molecular features and histological morphology, WHO reclassified grade IV GBM into several types of adult diffuse highest-grade gliomas (ADHGG) in 2021, such as IDH-mutant astrocytoma, oligodendroglioma with IDH-mutant and 1p19q co-deletion, and IDH-wild-type GBM. However, due to the high heterogeneity of ADHGG, more sophisticated molecular subtyping is still needed to distinguish the people with different prognosis and treatment response.

Immunotherapeutic approach such as immune-checkpoint inhibitors can effectively control the progression of various tumors, but has not achieved significant efficacy in ADHGG [9], which is likely caused by the unique immunosuppressive tumor microenvironment characterized by M2-polarized macrophages, T cell exhaustion, and production of specific cytokines [10]. Moreover, the biological causes of ADHGG invasion and treatment resistance are closely related to the immunosuppressive microenvironment [11]. Therefore, the identification of different immunotherapy-responsive subtypes based on the tumor microenvironment can potentially improve patient selection for treatment.

Cancer-associated fibroblast (CAF), as a vital component of the tumor immune microenvironment (TIME), plays an important role in extracellular matrix remodeling, cancer cell proliferation, metastasis, tumor angiogenesis, tumor stemness, immunosuppression and drug resistance [12–17]. Since there are no fibroblasts in the brain, it has not been clear whether fibroblasts exist in ADHGG for a long time [18]. However, cells expressing CAF markers were identified in ADHGG [19]. Recent studies revealed the existence of CAF in ADHGG through single-cell RNA sequencing and spatial transcriptomics, and found that they can promote tumor growth, and affect the prognosis and treatment response of patients [20,21]. At present, the functional implication of the association and interaction between ADHGG and CAF is poorly understood. Hence, CAFs provide a new perspective for the characterization and subtyping of ADHGG tumor immunosuppressive microenvironment.

In this study, we aimed to construct a classifier that can identify ADHGG subtypes with different CAF infiltration characteristics to predict patients' prognosis and responsiveness to anti-tumor therapy. We combined single-cell RNA sequencing and spatial transcriptomics data to characterize the CAF-infiltrating cellular landscape and identify CAF-associated signature markers in ADHGG. Based on this, we identified ADHGG with differential CAF infiltration characteristics and explored the association between CAF subtypes and the TIME, mutations, prognosis, clinical characteristics and treatment responss. Then, we constructed an artificial neural network model to accurately predict CAF subtypes in ADHGG. Finally, we also collected tissue samples from 6 patients with IDH mutation and 6 patients with IDH wildtype to verify that different CAF subtypes have distinct clinical characteristics and TIME. Taken together, our study provides a reference for the individualized treatment of ADHGG patients and the delineation of the immunosuppressive microenvironment of ADHGG.

2. Materials and methods

2.1. Data processing and annotation of scRNA-seq and stRNA-seq

Single-cell sequencing (scRNA-seq) data of 6 samples with ADHGG (gliomas of grade IV) in GSE141383, including 10502 cells and 22913 genes, were downloaded from TISCH database (http://tisch.comp-genomics.org/) [22]. The TISCH database has performed quality control and normalization of the data, and the "ScaleData" function was used to further standardize and scale the data. Based on the top 2000 hypervariable genes, the top 15 principal components were extracted by "RunPCA" function. According to the annotation results of TISCH database, all cells were divided into five clusters: Endothelial, Fibroblasts, Malignant, Mono/Macro, and Oligodendrocyte. Spatial transcriptomics sequencing (stRNA-seq) data downloaded from 10 × database (https://www.10xgenomics.com/cn/), which consists of 3468 cells, and 20950 genes. The "SCTransform" function was used to normalize the data. All regions were segmented into ST points based on hematoxylin-eosin (H&E) staining sections, and similar ST points were unsupervised clustered by the "FindNeighbors" and "FindClusters" functions, and fibroblast clusters were identified using COL1A1 and COL3A1 as markers. All scRNA-seq and stRNA-seq data were first converted into Seurat objects by the "Seurat" R package [23] before further analysis. Uniform manifold approximation and projection (UMAP) and t-distributed stochastic neighbor embedding (tSNE) were used to reduce the dimensionality of cells to a two-dimensional image for clustering and visualization [24].

2.2. Data analysis of scRNA-seq and stRNA-seq

The "FindAllMarkers" function of "Seurat" R package was used to find the key differential genes (KDEGs) whose expression levels in CAF cluster cells were significantly higher than that in other cluster cells in scRNA-seq data, and the p value was corrected by bonferroni multiple test. The screening criteria were adj. p.val <0.05 and avg. logFC >0.5, and expression had to be detected in at least 25 % of the cells. Next, KDEGs were screened for different single clusters, and the gene expression profiles of each cluster in scRNA-seq and stRNA-seq data were compared. Multimodal Intersection Analysis (MIA) was performed using the "phyper" function to calculate significant overlap degree of the same gene between clusters, and regions and key genes with high overlap degree with fibroblast cluster gene expression profiles were screened from stRNA-seq data [25]. The intersection of the key genes and KDEGs from scRNA-seq was defined as CAF key genes in ADHGG.

2.3. Pseudotime analysis

The "monocle2″ R package was used to perform pseudotime analysis of CAF cluster cells in the spatial transcriptome [26]. The analysis included three parts: to find the position of different CAF clusters in the cell differentiation trajectory and the transition relationship between them, to study the clustering of hypervariable genes in the pseudo-time series, and to study the expression patterns of CAF key genes in different "states". The screening criteria for hypervariable genes were mean expression ≥0.5 and dispersion_empirical≥1* dispersion_fit. The "plot_pseudotime_heatmap" function was used to display their dynamic expression.

2.4. Collection and processing of bulk RNA-seq data of ADHGG (gliomas of grade IV)

The ADHGG (gliomas of grade IV) cohort in the CGGA database had complete data on IDH mutation, 1p19q co-deletion, and MGMT promoter methylation status, including 139 stage ADHGG patients in the CGGA-325 cohort and 249 stage ADHGG patients in the CGGA-693 cohort, with a total of 388 ADHGG samples and 23258 expression profiles (Table 1). Clinical data and gene expression data in FPKM format were downloaded and converted to log2 (TPM+1) format. Expression profiles from CGGA-325 and CGGA-693 cohorts were combined and debatch-subtracted using the "combat" function of the "sva" R package. According to PCA analysis, 30 samples that still showed outliers after correcting the batch effect were deleted, and 358 samples were finally obtained as the test set. The mRNA expression profiles of 183 Rembrandt cohort samples and clinical data were downloaded from the CGGA website (http://www.cgga.org.cn/). The "TCGAbiolinks" R package was used to download TPM data and clinical data for 162 TCGA- ADHGG samples. The simple nucleotide variant data from the TCGA- ADHGG cohort were

Downloaded in maf format from the GDC database (https://gdc.cancer.gov) and used to calculate TMB for each patient. The formula was as follows: TMB (mut/mb) = total mutation amount/size of target coding area. Copy number variation (CNV) data were downloaded from the UCSC Xena (http://xena.ucsc.edu/) database.

3. Identification of CAF subtypes

Univariate COX regression analysis was used to identify key CAF genes significantly associated with disease prognosis. Based on the expression profiles of 16 CAF key genes, we used the "ConsensusClusterPlus" R package to perform unsupervised clustering of ADHGG patients in the CGGA cohort to identify different CAF clusters/subtypes. PCA and t-SNE were used to demonstrate the discriminability of CAF key gene expression profiles between different subtypes. Kaplan-Meier survival analysis was used to compare the overall survival (OS) of different subtypes. The "clusterRepro" R package calculates the "in-group proportion" (IGP) of clusters, which is a method to test the robustness of cluster classification [26], and IGP was calculated using the TCGA-ADHGG and Rembrandt cohorts as validation cohorts to verify the robustness of CAF subtype clustering. IGP values closer to 1 indicate higher agreement and more reliable clustering results.

3.1. Pathway analysis

The "clusterProfiler" R package was used to perform KEGG pathway enrichment analysis of KDEGs. The "AddModuleScore" function of the "Seurat" R package was used to score fibroblasts on cells from the integrated scRNA-seq and stRNA-seq data, and the "GSVA" R package was used to perform ssGSEA analysis based on HALLMARK gene set for each cell to explore the difference of pathway enrichment between cells with high and low fibroblast scores. The "GSVA" R package was also used to perform gene set variation analysis (GSVA) between CAF subtypes A and B with KEGG, GO, REACTOME and HALLMARK gene sets.

Table 1
Baseline Data Sheet for the Cohort of CGGA- ADHGG (gliomas of grade IV).

Characteristic	levels	N (%)
Age	<65 years old	327 (91.3 %)
	≥65 years old	31 (8.7 %)
Gender	Male	214 (59.8 %)
	Female	144 (40.2 %)
IDH_mutation_status	Mutant	85 (24.4 %)
	Wildtype	263 (75.6 %)
1p19q_codeletion_status	Codel	20 (5.6 %)
	Non-codel	334 (94.4 %)
MGMTp_methylation_status	Methylated	162 (51.6 %)
	Un-methylated	152 (48.4 %)
Therapy_status	Non TMZ + Non Radiotherapy	28 (8.4 %)
	Non TMZ + Radiotherapy	30 (9.1 %)
	TMZ + Non Radiotherapy	34 (10.3 %)
	TMZ + Radiotherapy	239 (72.2 %)

3.2. Tumor immune microenvironment (TIME) analysis

CIBERSORT [27], ssGSEA, MCPcounter algorithm [28] was used to analyze the infiltration of immune cells in different CAF subgroups of TIME. The "ESTIMATE" R package was used to calculate the StromalScore, ImmuneScore, and ESTIMATEScore between two CAF subtybes. ESTIMATEScore is the sum of StromalScore and ImmuneScore, which approximately represents the non-tumor component of TIME [29]. Furthermore, the differential expression of immune checkpoints and cytokines between the two CAF subtypes was analyzed and visualized as a heatmap by the "pheatmap" R package.

3.3. Tumor mutation analysis

The "maftools" R package [30] visualized the gene mutation data in maf format in the form of waterfall plot to construct the tumor mutation landscape of patients with different CAF subtypes. All patients were divided into high TMB group and low TMB group based on the best cutoff value. The association between CAF subtypes and TMB was explored by differential analysis and combined survival analysis. In addition, we depicted the gain and loss of CNV of CAF key genes by calculating their CNV frequencies. In addition, we counted the proportion of three genetic variations (IDH mutation, 1p19q co-deletion, and MGMT promoter methylation) in CAF subtypes. We used univariate and multivariate Cox regression to analyze the prognostic linkage between CAF subtypes and the three genetic variants, and explored the combined prognostic significance of CAF subtype and the three genetic variants by subgroup KaplanMeier survival analysis.

3.4. Analysis of treatment response

Taking "cgp2016″ as the reference dataset, we used the "pRRophetic" R package to predict the semi-inhibitory concentration (IC50) value of TMZ in ADHGG patients. In addition, based on the data in the cancer drug sensitivity genomics (GDSC2) (https://www.cancerrxgene.org/), "oncoPredict" R package was used to construct a ridge regression model and to calculate the IC50 value and the area under the curve (AUC) value of TMZ for each patient. The lower IC50 and AUC corresponded to a higher sensitivity to TMZ. Subgroup survival analysis depending on chemoradiotherapy response data in the CGGA-ADHGG cohort further revealed differences in the response of patients with different CAF subtypes to chemoradiotherapy. Then, we used cMAP algorithm to explore the potential therapeutic drugs and the corresponding mechanism of action of subtype A. According to The Cancer Immunome Atlas (TCIA) database (https://www.tcia.at/home), four immunophenoscores (IPS) revealed responsiveness to anti-PD-1 or anti-CTLA-4 therapy in the TCGA-ADHGG cohort. Depending on the Tumor Immune Dysfunction and Exclusion (TIDE) database (http://tide.dfci.harvard.edu/), we predicted the response to immunotherapy for patients in TCGA-ADHGG, CGGA-ADHGG, and Rembrandt cohorts, and calculated the TIDE score, Microsatellite Instability (MSI) score, and CAF infiltration score.

3.5. Construction of artificial neural network model (ANN)

The $|\log FC|>1$ and $p < 0.05$ as the screening criteria were used to obtain the differentially expressed genes between CAF subtypes A and B. Then, we used the "randomForest" R package to perform random forest (RF) algorithm to screen the subtype characteristic genes. The default number of iterations for RF is 100. The RF model was considered sufficiently robust when 500 trees were constructed. The genes were scored based on Gini coefficient, and scores greater than 4 were selected as modeling genes. Next, we compared the expression level of the modeling genes for a certain single sample with the median expression level for all samples. In subtype B up-regulated genes, the value was 1 if the expression level was above the median and 0 otherwise. In the subtype B down-regulated genes in contrast. The gene expression profiles of patients were transformed into [0,1] standardized "gene signatures". Finally, we constructed the ANN model using the "neuralnet" R package and visualized it through the "NeuralNetTools" R package [31]. Weight parameters between nodes in ANN model in Table S1. The number of hidden neuron layers was set to 4 (two-thirds of the number of input layers plus two-thirds of the number of output layers). The "pROC" R package was used to construct the ROC curve of the ANN, and the AUC of the ANN model was validated by the TCGA-ADHGG and Rembrandt cohorts. The distribution of five model genes at the single-cell level was explored based on the TISCH database.

3.6. Immunohistochemistry and multiplex immunofluorescence

We collected formalin-fixed, paraffin-embedded tissue sections of 12 ADHGG (gliomas of grade IV) patients with complete clinical and prognostic information after standardized surgery, radiotherapy and temozolomide (4–6 cycles) treatment in the Third Xiangya Hospital of Central South University from January 2017 to January 2023 for immunohistochemistry and multiple immunofluorescence detection (clinical information of the XY3_ADHGG cohort is detailed in Table S2). This work was approved by the Ethics Committee of the Third Xiangya Hospital (Ethics No.23793). Microglia are unique and important immune-related cells in ADHGG. Therefore, we speculated the infiltration level of M2 microglia is different between two CAF subtypes, and verified it by immunofluorescence. In brief, we deparaffinized and rehydrated paraffin-embedded tissue sections and then blocked endogenous peroxidase activity with 3 % hydrogen peroxide for 25 min at 25 °C. For immunohistochemistry, sections were first incubated at 4 °C with primary antibodies CD248(1:200, BOSS, China), FN1(1:200, HUABIO, China), COL3A1(1:200, PTG, USA), COL1A2(1:200, PTG, USA), COL1A1(1:200, CST, USA) overnight, followed by incubation with multimerized anti-rabbit IgG-HRP secondary antibody for 90 min at room temperature. Then, images were acquired with an optical microscope at a magnification of 20 × , a brown staining observed under the

microscope is considered positive, and the mean density (the ratio of the cumulative optical density and the area of the positive expression site under the visual field) of the images were calculated. For immunofluorescence, we detected three marker molecules: COL1A1(1:200, CST, USA), IBA1(1:300, Abcam, UK), CD206 (1:200, PTG, USA). We labeled the three antigens by cycling staining and performed incubation with primary and secondary antibodies. For each cycle, antibody labeling was performed after epitope repair and protein blocking. After cyclic staining, each slide was counterstained with DAPI for 10 min and viewed under a fluorescence

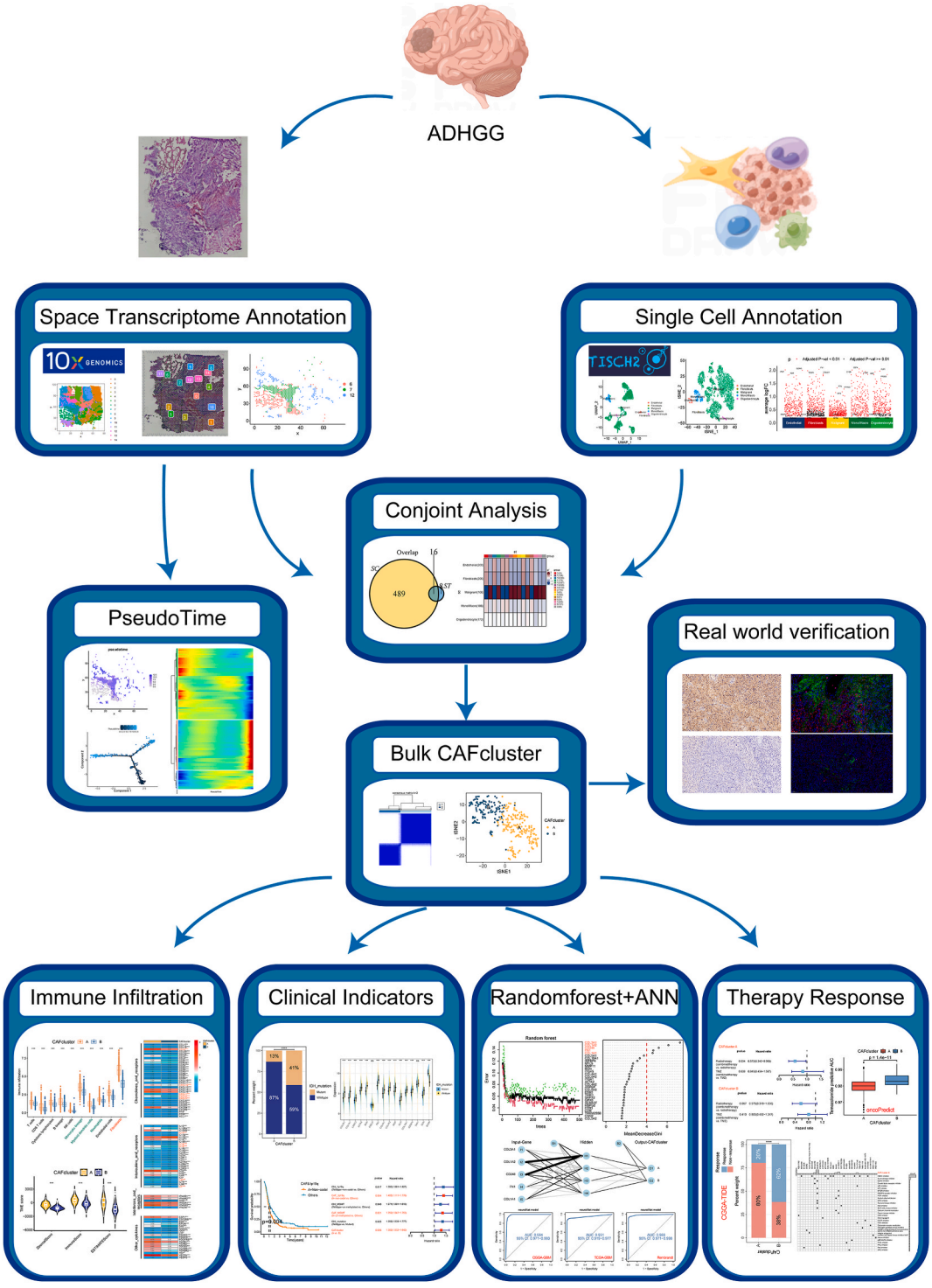

Fig. 1. The workflow of this study.

microscope, with images acquired at 20 × magnification. Post-imaging analysis and quantification were performed using Image-Pro-Plus. The ethical review Committee of the Third Xiangya Hospital, Central South University approved the project.

3.7. Statistical analysis

All bioinformatics analyses in this study were performed using R (v4.2.1) and Perl. Unless otherwise stated, the "limma" R package was used to perform the differential analyses, the Wilcoxon test was used to compare differences between two groups, and the Kruskal-Wallis test was used to compare differences between three or more groups. Spearman's correlation was used for correlation analyses. The R packages "survival" and "survivminer" were used for survival analysis. The default methods were used forKAplan-Meier survival and log-rank test. The student-t test was used to compare the two samples in the experimental part. Statistical data analysis was performed using GraphPad Prism 9.0. All statistical tests were bilateral, and p-values <0.05 were considered statistically significant.

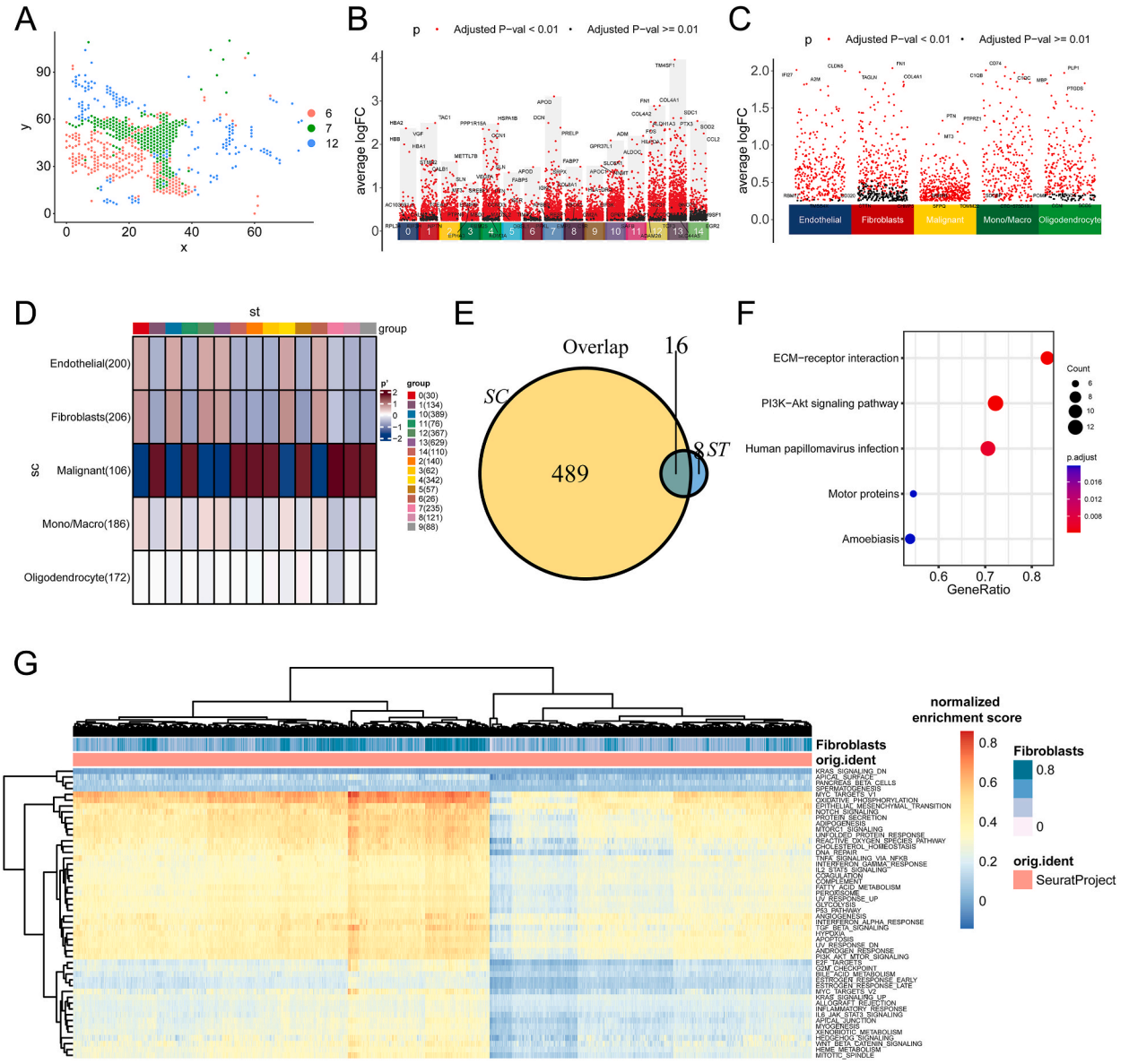

Fig. 2. Identification of key CAF genes and pathway exploration. (A) Spatial distribution of 6, 7 and 12 clusters (CAF clusters). (B) The Manhattan plot showed the KDEGs of 15 ST-clusters. (C) The Manhattan plot showed the KDEGs of five SC-clusters. (D) MIA established overlapping mapping of gene expression between scRNA-seq data and stRNA-seq data. The p' value was derived from the p-value of the hypergeometric distribution by negative logarithmic conversion and z-score normalization. The higher the p' value, the higher the overlap significance of gene expression profiles between the two clusters. (E) The Venn diagram identified 16 key CAF genes shared by scRNA-seq and stRNA-seq data. (F) KEGG analysis based on 505 KDEGs in the Fibroblasts cluster. (G) ssGSEA showed the enrichment pathways of cells with different CAF scores.

4. Results

4.1. Identification of CAF key genes based on scRNA-seq and stRNA-seq data

The workflow of this study is shown in Fig. 1. According to the annotation results of TISCH database, we reduce dimension and clustering by UMAP and t-SNE, and subdivided cells in the scRNA-seq data into five clusters: Endothelial, Fibroblasts, Malignant, Mono/Macro, and Oligodendrocyte (Figs. S1A and B). Next, we used unsupervised clustering to cluster similar ST points in stRNA-seq data, divided the H&E section image space into different 15 ST-clusters (Figs. S1C and D), and visualized the clustering of 15 ST-clusters by UMAP (Fig. S1E). We used COL1A1 and COL3A1 as markers of fibroblasts and found that they had significantly higher expression levels in clusters 6,7 and 12 (Fig. S1F), hence we annotated these as CAF clusters and identified the spatial distribution of CAF clusters in ST data (Fig. 2A). Next, we identified KDEGs in each cluster of stRNA-seq data (Fig. 2B) and scRNA-seq data (Fig. 2C), and evaluated the significance of the degree of overlap of gene expression in clusters of stRNA-seq data and scRNA-seq data by performing hypergeometric distribution with MIA. The results showed that among the CAF clusters identified previously, clusters 6 and 12 had significant overlap with the Fibroblasts cluster, while cluster 7 showed an overlap with the malignant cluster (Fig. 2D). Based on

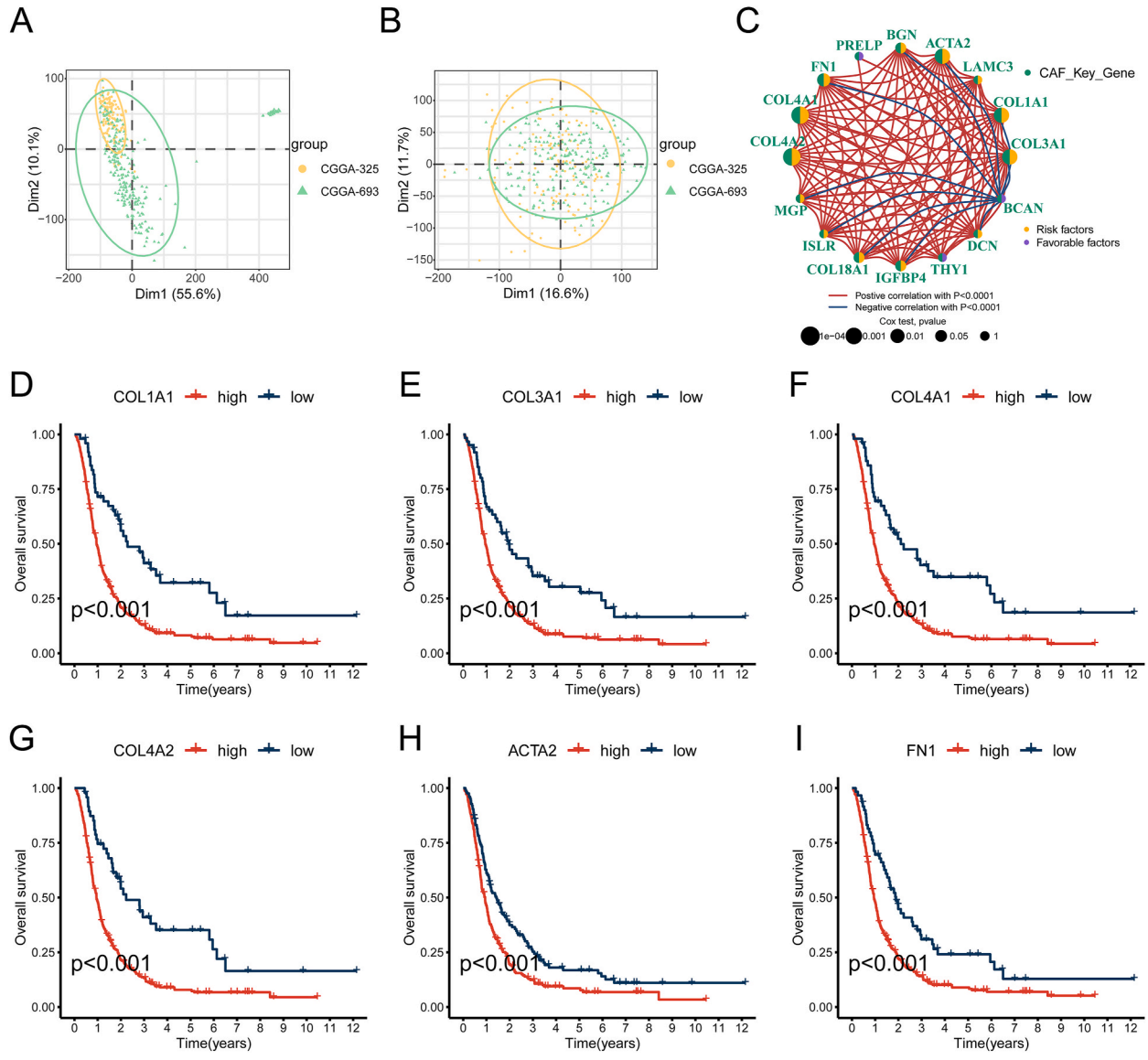

Fig. 3. Prognostic analysis of CAF key genes based on the CGGA-ADHGG cohort. (A, B) Fusion of CGGA-325 and CGGA-693 cohort data and removal of batch effects. (A) for PCA before removing batch effects, (B) for PCA post removing batch effects. (C) Correlation network of 16 CAF key genes. The line represents a correlation between genes, the sphere represents the Cox test of each gene. (D–I) K-M survival analysis of CAF key genes with great prognostic significance ($p \leq 0.001$).

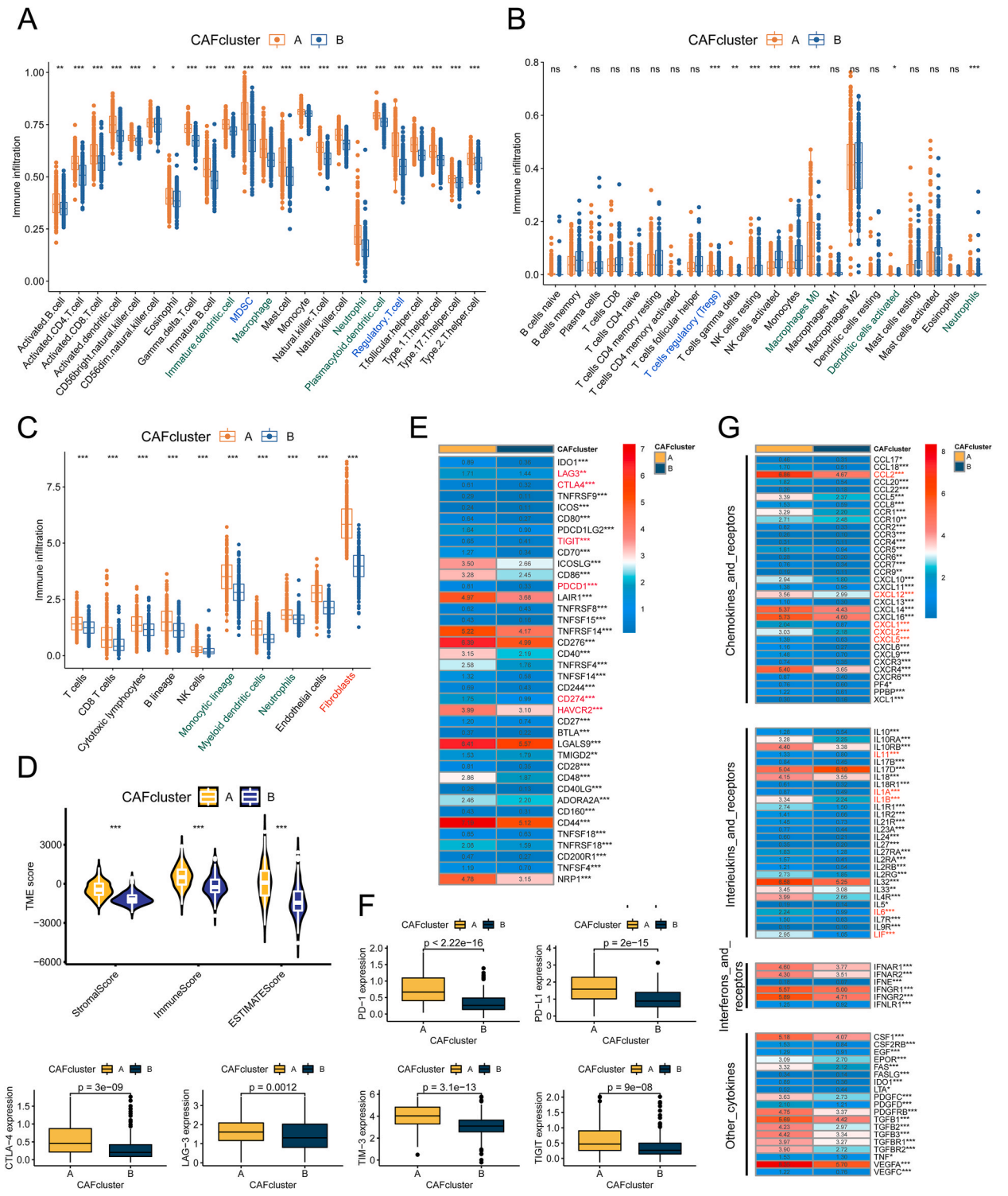

Fig. 4. TIME analysis based on CAFcluster. (A–C) The infiltration abundance of various immune cells in CGGA-ADHGG patients with different CAF subtypes were evaluated by ssGSEA (A), CIBERSORT (B) and MCPcounter (C) algorithms, respectively. Red represents CAF, blue represents immune suppressor cells associated with CAF, and green represents other immune cells associated with CAF. (D) Comparison of the stromal score, immune score and ESTIMATE score between patients in the A and B subtypes. (E, F) Expression differences of immune checkpoint genes between the two CAF subtypes. Six common immune checkpoint genes have higher levels in subtype A. (G) Expression differences of cytokine genes between the two CAF subtypes. Red represents cytokine genes associated with CAF. ns, no significant difference; *p < 0.05; **p < 0.01; ***p < 0.001.

MIA screening, we obtained 24 key genes from stRNA-seq data, and a total of 16 CAF key genes were obtained by intersection with 505 KDEGs screened from Fibroblasts cluster in scRNA-seq data, which were as follows: ACTA2, BCAN, BGN, COL18A1, COL1A1, COL3A1, COL4A1, COL4A2, DCN, FN1, IGFBP4, ISLR, LAMC3, MGP, PRELP, THY1 (Fig. 2E). Furthermore, KEGG pathway enrichment analysis was performed on 505 KDEGs in the Fibroblasts cluster, and the results showed that they were mainly enriched in ECM−receptor interaction and PI3K−Akt signaling pathway (Fig. 2F). Comprehensive ssGSEA analysis of KDEGs in stRNA-seq and scRNA-seq data showed that there were differences in enriched pathways between cells with high and low CAF scores, and the MYC_TARGETS_V1 pathway and OXIDATIVE_PHOSPHORYLATION pathway were enriched in cells with high CAF scores (Fig. 2G).

4.2. Pseudotime analysis of ST-CAF clusters

To explore the evolution of CAF clusters and associated hypervariable genes in the ADHGG tumor microenvironment in cell differentiation trajectories, we performed pseudotime analysis based on ST-CAF clusters. First, we show the pseudotime distribution landscape of ST-CAF clusters, in which the pseudotime value of cluster 6 was significantly lower than that of cluster 7 and 12 (Fig. S2A), representing the relatively early position of cluster 6 in cell development. We then deduced the cell differentiation trajectories of ST-CAF clusters and found a transition relationship from clusters 6 to clusters 7 and 12 (Figs. S2B and C). Finally, we screened the hypervariable genes within the ST-CAF cluster, and the heat map showed the presence of three dynamic expression patterns during cell development (Fig. S2D), which may play a key role in the differentiation and evolution of CAF clusters.

4.3. Comprehensive analysis of CAF key genes

We integrated the gene expression profiles of ADHGG patients in CGGA325 and CGGA693 cohorts, and the results of PCA showed that the batch effect of 358 sample gene expression profiles was reduced to an acceptable range (Fig. 3A and B). We performed univariate COX regression analysis on 16 CAF key genes and identified 6 key genes with prognostic significance: COL1A1, COL3A1, COL4A1, COL4A2, ACTA2 and FN1 ($p \leq 0.001$, Fig. 3C). Kaplan-Meier survival analysis showed that patients with higher expression of these six genes had significantly lower OS (Fig. 3D–I). We further used the “monocle” algorithm to cluster the cells in the stRNA-seq into five “states”, representing five different stages on the cell differentiation trajectory. We found that these six CAF key genes had highly similar expression patterns during cell development (Fig. S3).

4.4. Identification of CAF subtypes

Unsupervised clustering of patients in the CGGA-ADHGG cohort based on the expression of 16 key CAF genes divided patients into CAF subtypes A and B (Fig. S4A). In addition to PRELP and BCAN, the expression levels of the remaining CAF key genes in subtype A were significantly higher than those in subtype B ($p < 0.001$, Fig. S4B). The results of t-SNE and PCA showed that the expression of CAF key genes in patients with different CAF subtypes showed identifiable differences (Figs. S4C and D). Survival analysis displayed that the prognosis of patients with subtype B was significantly better than that of subtype A ($p < 0.05$, Fig. S4E). We used GSVA to identify differences in pathway activities in patients with two CAF subtypes from KEGG, GO, Reactome, and HALLMARK, and found that patients with subtype B showed an enrichment of immune-related pathways, such as T CELL PROLIFERATION, B CELL RECEPTOR SIGNALING PATHWAY and INFLAMMATORY RESPONSE (Fig. S5). In addition, we found that clustering in the TCGA-ADHGG cohort and the Rembrandt cohort had a high IGP (IGP >0.8, Figs. S6A and B), suggesting a great robustness in the identification of CAF subtypes. In the TCGA-ADHGG cohort (Figs. S6C–E) and Rembrandt cohort (Figs. S6F–H), the expression of key CAF genes was highly similar to those in the CGGA cohort, and the infiltration level of fibroblasts was markedly higher in subtype A than in subtype B.

4.5. Evaluation of tumor immune microenvironment based on CAFcluster

TIME is closely related to tumor progression, recurrence and response to immunotherapy. Immunotherapy is a promising treatment strategy for aggressive brain tumors [32]. We evaluated the infiltration levels of immune cells in ADHGG patients by ssGSEA (Fig. 4A), CIBERSORT (Fig. 4B), and MCPcounter (Fig. 4C). The results showed that patients with CAF subtype A had a significantly higher level of fibroblast infiltration and closely related immune cell infiltration, including Tregs, MDSCs, macrophages, neutrophils and dendritic cells enriched by cytokine regulation. ESTIMATE analysis showed that patients with subtype A had higher StromalScore, ImmuneScore and ESTIMATEScore compared with subtype B (Fig. 4D). CAFs can promote the expression of programmed cell death protein 1(PD1) and cytotoxic T-lymphocyte-associated protein 4 (CTLA-4) on activated T cells and PDL-1 on tumor cells, forming an immunosuppressive microenvironment. We analyzed the differences in the expression of immune checkpoint genes (ICGs) in different CAF subtypes, and found that the expression level of ICGs in patients with subtype A was generally higher than that in subtype B (Fig. 4E), including PD-1, PD-L1, CTLA-4, LAG3, TIM3, and TIGIT (Fig. 4F). Cytokines are important regulators of TIME. We also explored the expression of cytokines in patients with different ADHGG CAF subtypes, and our results showed that subtype A had higher levels of cytokine expression (Fig. 4G).

4.6. Tumor genetic variation analysis was based on CAFcluster

Tumor mutations affect the prognosis and treatment effect of ADHGG patients, especially IDH mutations. We compared the gene mutation landscape of patients with different CAF subtypes and found that the frequency of IDH1 and IDH2 mutations in patients with

subtype A was 0, which was significantly lower than that in patients with subtype B (Figs. S7A–B). We further explored the association of CAF subtypes with TMB and found that subtype B had a significantly higher TMB (Fig. S7C). Survival analysis indicated that ADHGG patients in lower TMB had lower OS (Fig. S7D), and patients with low TMB combined with subtype A had the worst prognosis (Fig. S7E). Through CNV analysis, we concluded that CAF key genes all had different degrees of CNV gain and loss, among which PRELP had the highest frequency of CNV gain, while ACTA2 had the highest CNV loss frequency (Fig. S7F). Fig. S3G shows the CNV gain and loss landscape of CAF key genes and their location on the chromosome. Apart from IDH mutation, 1p19q co-deletion and MGMT promoter methylation are also important genetic variants in ADHGG, which affect clinical decision making. We found that the proportion of IDH mutation and 1p19q co-deletion was significantly lower in subtype A than in subtype B, while the proportion of MGMT promoter methylation was not significantly different between the two subtypes (Figs. S8A–C). Meanwhile, patients grouped according to IDH mutation and 1p19q codeletion status showed similar differences in CAF key gene expression profiles (Figs. S8D–E) and fibroblast infiltration levels (Figs. S8F–G) with those grouped according to CAF subtypes. COX regression analysis showed that IDH mutation, 1p19q codeletion, and CAF type B were all factors associated with improved prognosis in ADHGG patients (Fig. 5A), but there may be a prognostic linkage between CAFcluster and the three genetic variants (Fig. 5B). More closely, stepwise subgroup survival analysis revealed A significant prognostic difference between subtype A and subtype B only in the population without 1p19q co-deletion or MGMT promoter methylation (Fig. 5C–E). In the case of known CAF classification of patients, only the detection of 1p19q co-deletion status in patients with subtype A has prognostic significance (Fig. 5F–H). Combined with the previous results, we hypothesized that there might be an intimate relation between CAFcluster and IDH mutations. Furthermore, we compared the prognostic significance of CAFcluster and IDH mutations. The results suggested that the combination of 1p19q non-codel and MGMTp unmethylated could identify the patients with worse prognosis regardless of subtype A or IDH wild-type (Figs. S9A–D). Moreover, CAFcluster has greater significance in joint prediction of prognosis than IDH (Fig. S9E).

4.7. Analysis of therapeutic response based on CAFcluster

Radiotherapy and TMZ chemotherapy are the cornerstones of ADHGG treatment. Both “pRRophetic” and “oncoPredict” algorithms showed that compared with subtype B, subtype A patients had lower IC50 and AUC values of TMZ (Fig. 6A–C), suggesting that subtype A had better sensitivity to TMZ. Survival analysis based on the CGGA cohort suggested that patients receiving chemotherapy combined with radiotherapy had a higher OS (Fig. 6D). To explore whether combined chemoradiotherapy had a significant survival benefit compared with radiotherapy or chemotherapy alone, Cox regression was performed to calculate hazard ratios for risk quantification. The results showed that for patients with subtype A, chemoradiotherapy had a significant benefit compared with radiotherapy alone, but no survival benefit compared with TMZ alone. In patients with subtype B, there was no survival benefit of chemoradiotherapy versus radiotherapy or chemotherapy alone (Fig. 6E). In addition, we used the cMAP algorithm to identify various HDAC inhibitors that may be potential therapeutic agents for patients with subtype A (Fig. 6F). The TCIA database predicted that patients with subtype A had lower IPS and IPS-CTLA4 blocker than those with subtype B (Fig. 6G). Consistent results were obtained in the CGGA-TIDE, TCGA-TIDE, and Rembrandt-TIDE cohorts. Patients with subtype A had a significantly lower response to immunotherapy than those with subtype B (Fig. 7A). Compared with subtype B patients, the CAF score and TIDE score were significantly higher, and the MSI score was significantly lower (Fig. 7B–D).

4.8. Construction of ANN for distinguishing CAFcluster

In order to more easily and accurately identify CAF subtypes in a small number of samples or individual ADHGG patients, an ANN model was constructed. Firstly, we obtained 5774 differentially expressed protein-coding genes between the two CAF subtypes by differential analysis (Fig. 8A). Subsequently, we screened five subtype-related differential feature genes by random forest algorithm: COL3A1, COL1A2, CD248, FN1 and COL1A1 (Fig. 8B and C), and finally constructed an ANN model based on the characteristic genes (Fig. 8D). In the CGGA-ADHGG, TCGA-ADHGG, and Rembrandt cohorts, the predicted AUCs of the ANN model were 0.984, 0.951, and 0.988, respectively (Fig. 8E). All five model genes were expressed predominantly on fibroblasts, with low levels of expression on the remaining cells (Fig. S10).

4.9. Validation of CAF clustering in ADHGG clinical cohort

Formalin-fixed, paraffin-embedded tissue sections of 12 ADHGG patients from the Third Xiangya Hospital of Central South University from January 2017 to January 2023 were collected for immunohistochemistry and multiple immunofluorescence assays to evaluate the stability of ANN classification and the infiltration level of M2 microglia in different subtypes. The expression levels of CD248, COL1A1, COL1A2, COL3A1, and FN1 in 12 patients were detected by immunohistochemistry. According to the quantitative results of immunohistochemistry of CAF key genes, the gene expression profile of patients was transformed into [0,1] standardized “gene signature”, and the patients were classified by ANN model. Nine patients were classified as type A and three as type B. We found that CAF subtype A had higher expression levels of CAF key genes (Fig. 9A) and lower rate of IDH1 mutation (Fig. 9B) than CAF subtype B in our cohort. Compared with subtype B, subtype A had a worse treatment response, with 8 of 9 patients having disease progression (PD: 89 %) (Fig. 9C). Next, we used multiple immunofluorescence staining to evaluated the level of infiltration of M2 microglia in different CAF subtypes, and we observed that subtype A had a higher level of M2 microglia (Fig. 9D).

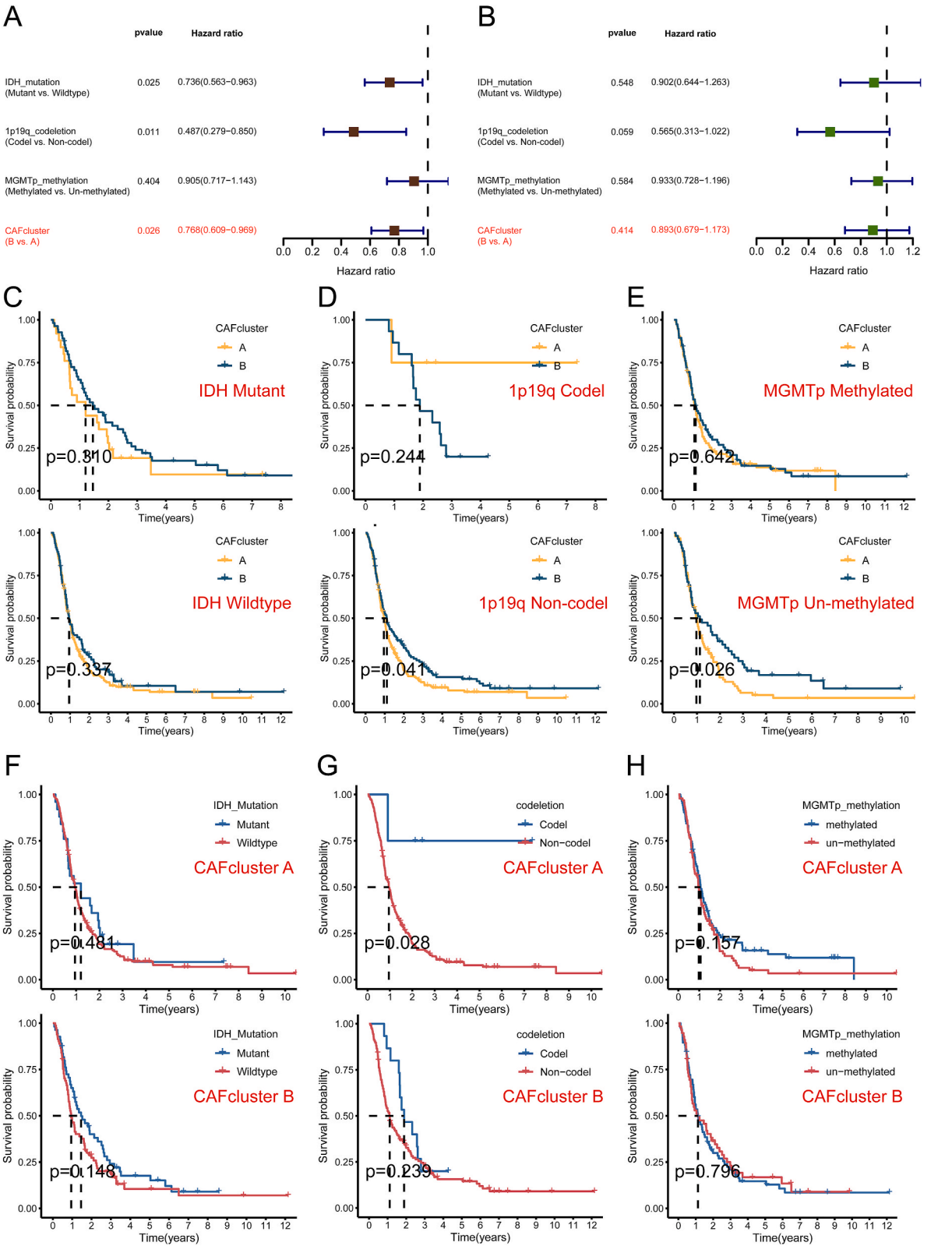

(caption on next page)

Fig. 5. Prognostic analysis combined CAFcluster with important genetic variants in ADHGG. (A, B) Cox regression analysis related with CAFcluster, IDH mutation, 1p19q co-deletion and MGMT promoter methylation: univariate (A) and multivariate (B). (C–E) Combined survival analysis by first detecting genetic variants and then detecting CAFCluster: IDH mutation (C), 1p19q co-deletion (D) and MGMT promoter methylation (E). (F–H) Combined survival analysis by first detecting CAFCluster and then detecting genetic variants: IDH mutation (F), 1p19q co-deletion (G) and MGMT promoter methylation (H).

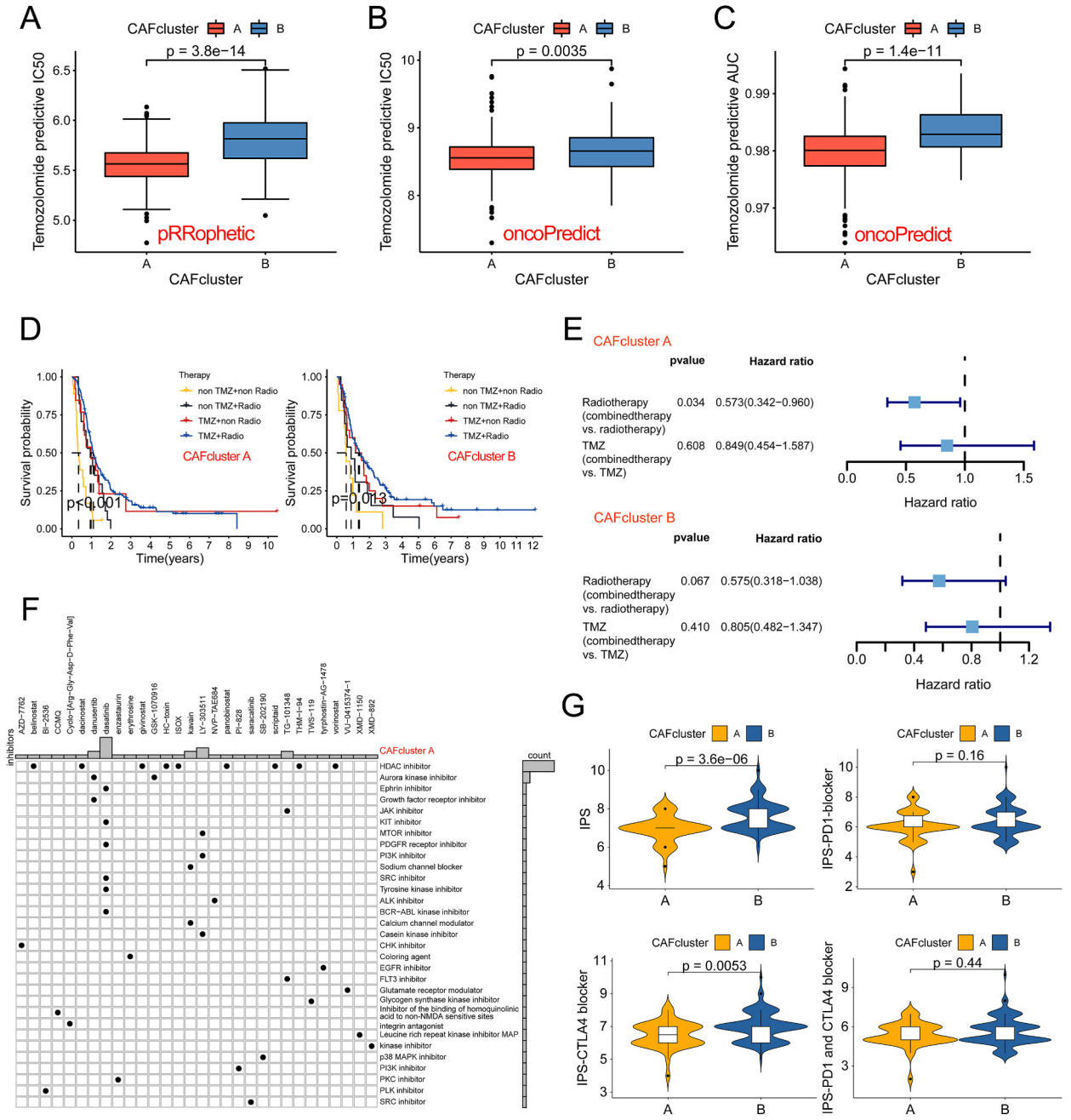

Fig. 6. Treatment responsiveness analysis based on CAFcluster. (A–C) Temozolomide sensitivity analysis in patients with ADHGG by using different algorithms and data: The pRRophetic algorithm was performed to predict IC50 based on the cgp2016 dataset (A), the oncoPredict algorithm was performed to predict IC50 (B) and AUC (C) based on the GDSC2 dataset. (D) Survival analysis revealed the prognostic difference among different treatment status with TMZ and radiotherapy in two CAF subtypes. (E) Univariate Cox regression analysis explored whether the combination of radiotherapy and TMZ was more beneficial than treatment alone in two CAF subtypes. (F) Potential therapeutic drugs and mechanisms for patients with CAF subtype A were explored based on the cmap algorithm. (G) Comparsion of four kinds of IPS between two CAF subtypes based on TCIA database.

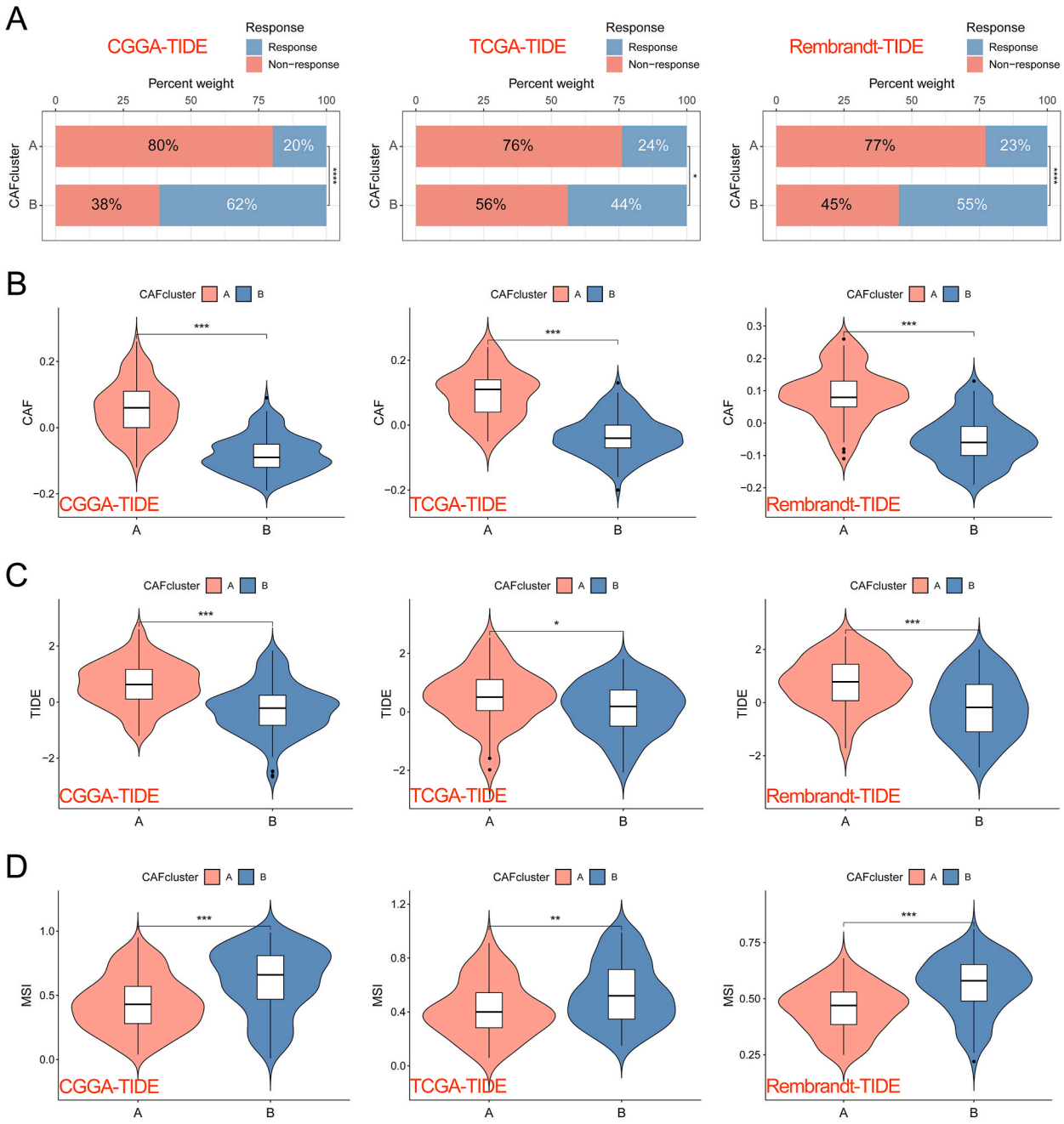

Fig. 7. Predictive immunotherapy responsiveness of ADHGG patients based on TIDE algorithm. (A) The response ratio of patients with different CAF subtypes to immunotherapy was predicted and compared based on three independent cohorts. (B–D) The CAF score (B), TIDE score (C) and MSI score (D) of patients with different CAF subtypes were predicted and compared based on three independent cohorts. *$p < 0.05$; **$p < 0.01$; ***$p < 0.001$; ****$p < 0.0001$.

5. Discussion

As a pivotal component of the tumor microenvironment, CAFs are associated with metastasis and immunosuppression of many solid tumors. Recent study have confirmed the presence of CAF in ADHGG [20], which may help us to further understand the immunosuppressive tumor microenvironment of ADHGG and provide more accurate treatment decisions.

In this study, we first identified CAF and corresponding key genes in ADHGG based on scRNA-seq and stRNA-seq data, which share similar spatiotemporal expression characteristics during ADHGG tumorigenesis and progression. Almost all of them are prognostic risk factors for ADHGG patients. According to the CAF key genes, ADHGG patients were divided into subtypes A and B. Patients with

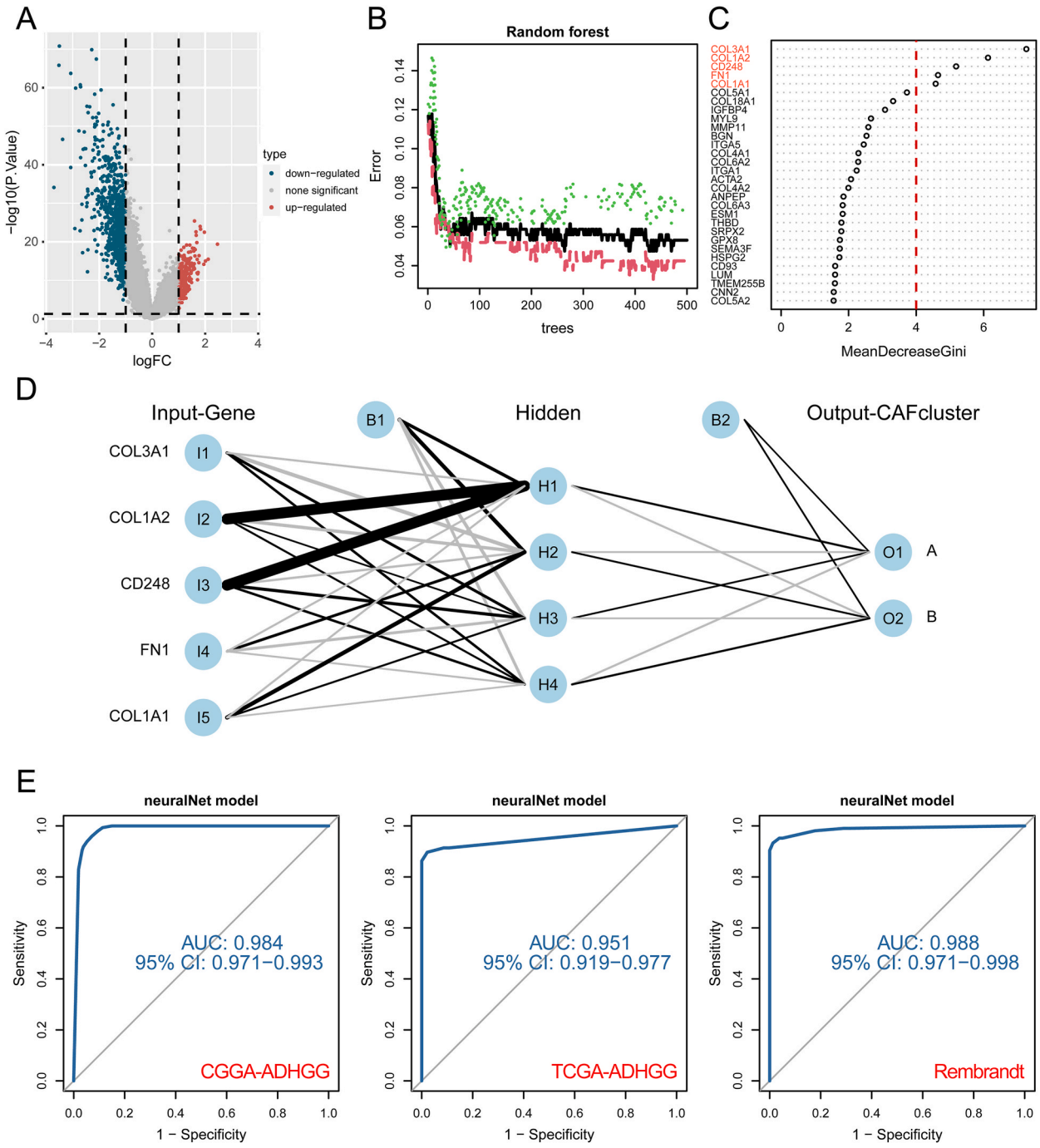

Fig. 8. Construction and validation of ANN models for identification of CAF subtypes. (A) Difference analysis identified differential genes of subtype B compared with subtype A. (B) The relationship between the number of trees and model error in random forest. The model has the smallest error when the number of trees is 264. (C) The genes whose importance score was greater than 4 based on Gini coefficient method were selected as model genes. (D) Schematic diagram of ANN model, where the number of hidden layers is 4. Five model gene expression profiles of patients were input in the input layer, and CAF subtypes of patients were finally output according to the calculation of weight coefficients. (E) The ROC of ANN models in three independent cohorts was used to verify the predictive efficacy.

different CAF subtypes have different CAF related biological characteristics and prognosis.

Further, we performed CIBERSORT, ssGSEA, MCP counter and ESTIMATE algorithms to compare the differences in the tumor immune microenvironment of ADHGG patients with different CAF subtypes. Compared with the subtype B, subtype A showed higher expression of CAF related genes and also higher levels of immune cell infiltration, including Tregs, MDSCs, macrophages, neutrophils

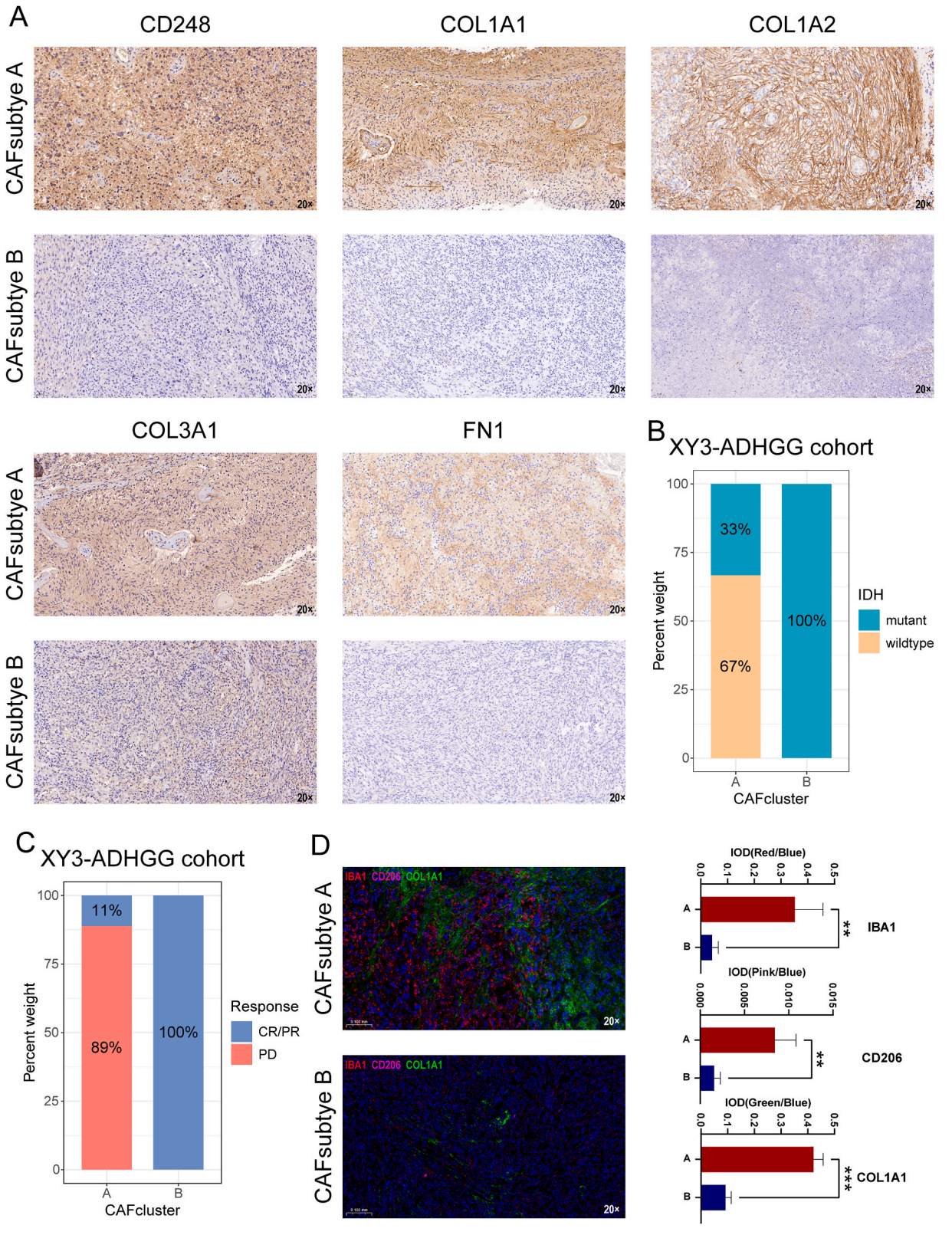

(caption on next page)

Fig. 9. Validation of real-world cohort based on ANN model. (A) By inputting the immunohistochemical score of the five model genes into the ANN model, the XY3-ADHGG cohort was identified as two CAF subtypes. Representative immunohistochemical image of CD248, COL1A1, COL1A2, COL3A1, and FN1 in different CAF subtypes, the magnification was 20 × . (B) The IDH mutant proportion of patients with different CAF subtypes was compared based on the XY3-ADHGG cohort. (C) The response ratio of patients with different CAF subtypes to systemic antitumor therapy was compared based on the XY3-ADHGG cohort. (D) Immunofluorescence was used to investigate the differences of COL1A1(Green), IBA1(Red) and CD206(Pink) signal enrichment in TIME of patients with different CAF subtypes, the magnification was 20 × , "_" represent 0.1 mm.

and dendritic cells, which are closely associated with CAF. In addition, subtype A showed an enrichment of cytokines and inflammatory factors, more matrix components deposition, and significantly upregulated expression of ICGs including PD-1,PD-L1 and CTLA-4. The immune microenvironment of high CAF is usually in an inflammatory state, which will secrete a large number of inflammatory factors and cytokines, attract macrophages, MDSC, neutrophils and other monocytic myeloid cells and Treg cells, promote tumor growth and form immunosuppression [33]. CAFs can also inhibit immunity by hindering the infiltration activity of T cells through matrix fibrosis. Moreover, CAF promote the expression of PD1 and CTLA4 on activated T cells and PDL1 on tumor cells, and promote immune escape [34]. There is a substantial exhaustion of T cells in ADHGG [35]. Although the infiltration level of T cells is high in patients with subtype A, they present a non-functional "exhaustion" state due to the inhibitory effect of immunosuppressive cells. We further explored whether there were differences in the response to immunotherapy in ADHGG patients with different CAF subtypes. Our analysis of the CGGA, TCGA and Rembrandt cohorts all showed that patients with subtype A had a higher CAF invasion level, a lower immunotherapy response rate, a higher TIDE score and a lower MSI score than patients with subtype B. The results of TCIA database showed that subtype A had lower IPS and was less responsive to ICIs, especially anti-CTLA4 inhibitors. The above results suggest that CAF subtype A may regulate the formation of immunosuppressive tumor microenvironment to reduce the responsiveness of immunotherapy.

Gene mutation is not only a crucial cause of ADHGG, but also a meaningful prognostic prediction and therapeutic biological behavior. IDH mutation, 1p19q codeletion and MGMT promoter methylation are clinically important gene mutation detection indicators in ADHGG. IDH mutation and 1p19q codeletion are associated with better prognosis and sensitivity to chemoradiotherapy. MGMTp methylation status can be used to predict the sensitivity to TMZ treatment. Our analysis found that patients of CAF subtype B with better prognosis have a higher frequency of IDH mutation and 1p19q codeletion, and patients with IDH mutations and 1p19q codeletions have similar CAF related gene expression and CAF infiltration level as patients with B subtype. IDH1 mutant ADHGG stem cells can secrete G-CSF to improve the efficacy of immunotherapy [36], which may partly explain the better immune response and prognosis of subtype B. Cox regression analysis revealed the prognostic linkage between CAF subtype, IDH mutation and 1p19q co-deletion. The subtypes prognostic analysis showed that CAF subtype could identify more combined prognostic risk populations than IDH mutation. Furthermore, the higher frequency of IDH mutations in subtype B was validated in TCGA mutation data and real-world cohort. We also explored the association between CAF subtype and TMB, subtype A patients with low TMB had the worst prognosis.

Radiotherapy is an important local treatment for ADHGG patients, and TMZ is the first-line therapy option for newly diagnosed ADHGG patients. Compared with chemotherapy or radiotherapy alone, radiotherapy combined with TMZ chemotherapy show superior outcome in ADHGG patients [1]. In subtype A, compared with radiotherapy alone, the combination of radiotherapy and chemotherapy showed a significant benefit, but compared with TMZ chemotherapy alone, the benefit is not significant, which may be related to CAF leading to radiotherapy resistance [37] and subtype A being more sensitive to TMZ chemotherapy. However, in subtype B with low infiltration of CAF, chemoradiotherapy has no significant benefit compared with radiotherapy and chemotherapy alone, suggesting that subtype B radiotherapy or chemotherapy alone may be sufficient. We utilized cMAP algorithm to identify various HDAC inhibitors as potential therapeutic drugs for patients with subtype A. HDAC inhibitors can effectively inhibit the release of tissue repair cells, such as macrophages, which are extremely critical to fibroblast proliferation and collagen synthesis and degradation [38, 39]. With the deepening of our understanding of the tumor-promoting role of CAF, the therapeutic idea of targeting CAF to inhibit tumor progression and enhance anti-tumor immunity has also emerged [40]. These methods mainly include targeting key signaling molecules related to CAFs, normalizing or reprogramming CAF to a resting state, and directly or indirectly depleting CAFs through immunotherapy or transgenic methods [41]. Currently, there are some clinical or preclinical studies of potential drugs targeting CAFs, such as multi-receptor somatostatin analogue pasireotide SOM230 in pancreatic cancer [42]. Blockade of PDGFR signaling in CAF by kinase inhibitor imatinib can significantly reduce the production of FGF2 and FGF7, thereby inhibiting tumor angiogenesis and cancer cell proliferation [43]. Vaccination against FAP antigen in CAF may be an effective way for cancer immunotherapy [44]. There have been no drug reports about CAF in ADHGG, but targeting CAF may be a promising treatment for ADHGG and bring greater therapeutic benefit to patients with CAF subtype A.

ConsensusClusterPlus clustering has two obvious disadvantages: the clustering results are unstable when the sample size is small; More target genes need to be tested to identify subtypes, which limits its clinical application. To address this issue, we constructed an ANN classifier based on five CAF genes, which showed high prediction performance in three independent cohorts. Finally, we applied the ANN model using our own cohort, and we found that subtype A had higher CAF gene expression and more CAF and M2-type microglia infiltration in its TIME. In addition, subtype A patients have lower IDH mutation rate and worse treatment response, which is consistent with our previous results, proving that our ANN model has certain clinical application value and may provide help for prognosis prediction and treatment decision-making of ADHGG patients. In summary, the establishment of CAF subtypes can help us to judge the prognosis and treatment response of patients, and develop more accurate and scientific treatment strategies. CAF may act as a bridge factor to link the crosstalk between IDH mutations and the immune microenvironment in ADHGG.

6. Conclusion

This study reveals the role of CAF in ADHGG. The importance of prognosis, IDH mutations status, responsiveness to immunotherapy, radiotherapy and temozolomide in CAF and ADHGG patients was demonstrated. We further constructed an artificial neural network model based on five CAF genes which could identify CAF subtypes of ADHGG patients and validated the classifier in a real-world cohort, which may improve clinical decision-making of ADHGG.

Funding

This work was supported by the Funds for International Cooperation and Exchange of the National Natural Science Foundation of China (GZ1699), key research and development projects in Hunan Province (2022SK2022), the science and technology innovation Program of Hunan Province (2020RC4011), the Hunan Province Science and Technology Talent Promotion Project (2019TJ-Q10), Scientific research project of Hunan Provincial Health Commission (202209034683), Young Scholars of "Furong Scholar Program" in Hunan Province, Central South University Research Programme of Advanced Interdisciplinary Studies (2023QYJC017), and the Wisdom Accumulation and Talent Cultivation Project of the Third xiangya hosipital of Central South University (BJ202001).

Ethics approval and consent to participate

This work was approved by the Ethics Committee of the Third Xiangya Hospital (Ethics No.23793).

Consent for publication

Not applicable.

Data availability statement

The data supporting this study's findings are available in the methods and/or supplementary material of this article. The complete original data and code can be downloaded from: https://www.jianguoyun.com/p/DYimWrwQyIXODBiun8QFIAA.

CRediT authorship contribution statement

Ganghua Zhang: Writing – original draft, Methodology. **Panpan Tai:** Writing – review & editing, Writing – original draft, Formal analysis. **Jianing Fang:** Formal analysis. **Zhanwang Wang:** Data curation. **Rui Yu:** Writing – original draft, Formal analysis. **Zhijing Yin:** Formal analysis. **Ke Cao:** Conceptualization.

Declaration of competing interest

The authors declare the following financial interests/personal relationships which may be considered as potential competing interests:Ke Cao reports financial support was provided by the Funds for International Cooperation and Exchange of the National Natural Science Foundation of China. Ke Cao reports financial support was provided by key research and development projects in Hunan Province. Ke Cao reports financial support was provided by Scientific research project of Hunan Provincial Health Commission. Ke Cao reports financial support was provided by the science and technology innovation Program of Hunan Province. Ke Cao reports financial support was provided by the Hunan Province Science and Technology Talent Promotion Project. If there are other authors, they declare that they have no known competing financial interests or personal relationships that could have appeared to influence the work reported in this paper.

Acknowledgments

We thank Professor tianzuo Zhan of the Department of Medicine II, Medical Faculty Mannheim of Heidelberg University, for language assistance with this paper.

Appendix A. Supplementary data

Supplementary data to this article can be found online at https://doi.org/10.1016/j.heliyon.2024.e34526.

References

[1] A.C. Tan, D.M. Ashley, G.Y. López, M. Malinzak, H.S. Friedman, M. Khasraw, Management of glioblastoma: state of the art and future directions, CA A Cancer J. Clin. 70 (2020) 299–312.

[2] P.Y. Wen, M. Weller, E.Q. Lee, B.M. Alexander, J.S. Barnholtz-Sloan, F.P. Barthel, et al., Glioblastoma in adults: a Society for Neuro-Oncology (SNO) and European Society of Neuro-Oncology (EANO) consensus review on current management and future directions, Neuro Oncol. 22 (2020) 1073–1113.
[3] L. Marenco-Hillembrand, O. Wijesekera, P. Suarez-Meade, D. Mampre, C. Jackson, J. Peterson, et al., Trends in glioblastoma: outcomes over time and type of intervention: a systematic evidence based analysis, J. Neuro Oncol. 147 (2020) 297–307.
[4] N. Goffart, A. Lombard, F. Lallemand, J. Kroonen, J. Nassen, E. Di Valentin, et al., CXCL12 mediates glioblastoma resistance to radiotherapy in the subventricular zone, Neuro Oncol. 19 (2017) 66–77.
[5] Q. Chen, W. Wang, Z. Wu, S. Chen, X. Chen, S. Zhuang, et al., Over-expression of lncRNA TMEM161B-AS1 promotes the malignant biological behavior of glioma cells and the resistance to temozolomide via up-regulating the expression of multiple ferroptosis-related genes by sponging hsa-miR-27a-3p, Cell Death Dis. 7 (2021) 311.
[6] M.S. Lam, J.J. Aw, D. Tan, R. Vijayakumar, H.Y.G. Lim, S. Yada, et al., Unveiling the influence of tumor microenvironment and spatial heterogeneity on temozolomide resistance in glioblastoma using an advanced human in vitro model of the blood-brain barrier and glioblastoma, Small 19 (2023) 2302280.
[7] S.Y. Lee, Temozolomide resistance in glioblastoma multiforme, Genes Dis 3 (2016) 198–210.
[8] L. Montella, N. Del Gaudio, G. Bove, M. Cuomo, M. Buonaiuto, D. Costabile, et al., Looking beyond the glioblastoma mask: is genomics the right path? Front. Oncol. 12 (2022) 926967.
[9] D.A. Reardon, A.A. Brandes, A. Omuro, P. Mulholland, M. Lim, A. Wick, et al., Effect of nivolumab vs bevacizumab in patients with recurrent glioblastoma: the CheckMate 143 phase 3 randomized clinical trial, JAMA Oncol. 6 (2020) 1003–1010.
[10] D. Kreatsoulas, C. Bolyard, B.X. Wu, H. Cam, P. Giglio, Z. Li, Translational landscape of glioblastoma immunotherapy for physicians: guiding clinical practice with basic scientific evidence, J. Hematol. Oncol. 15 (2022) 80.
[11] D.F. Quail, J.A. Joyce, The microenvironmental landscape of brain tumors, Cancer Cell 31 (2017) 326–341.
[12] U. Schwartz, M. Llamazares Prada, S.T. Pohl, M. Richter, R. Tamas, M. Schuler, et al., High-resolution transcriptomic and epigenetic profiling identifies novel regulators of COPD, EMBO J. 42 (2023) e111272.
[13] Y. Li, H. Zheng, Y. Luo, Y. Lin, M. An, Y. Kong, et al., An HGF-dependent positive feedback loop between bladder cancer cells and fibroblasts mediates lymphangiogenesis and lymphatic metastasis, Cancer Commun. (2023).
[14] J. Zhuang, L. Shen, M. Li, J. Sun, J. Hao, J. Li, et al., Cancer-associated fibroblast-derived miR-146a-5p generates a niche that promotes bladder cancer stemness and chemoresistance, Cancer Res. 83 (2023) 1611–1627.
[15] G.-Q. Zhu, Z. Tang, R. Huang, W.-F. Qu, Y. Fang, R. Yang, et al., CD36+ cancer-associated fibroblasts provide immunosuppressive microenvironment for hepatocellular carcinoma via secretion of macrophage migration inhibitory factor, Cell Discov 9 (2023) 25.
[16] Y. Chen, K.M. McAndrews, R. Kalluri, Clinical and therapeutic relevance of cancer-associated fibroblasts, Nat. Rev. Clin. Oncol. 18 (2021) 792–804.
[17] D. Yang, J. Liu, H. Qian, Q. Zhuang, Cancer-associated fibroblasts: from basic science to anticancer therapy, Exp. Mol. Med. 55 (2023) 1322–1332.
[18] V.S. LeBleu, E.G. Neilson, Origin and functional heterogeneity of fibroblasts, Faseb. J. 34 (2020) 3519–3536.
[19] A. Clavreul, C. Guette, R. Faguer, C. Tétaud, A. Boissard, L. Lemaire, et al., Glioblastoma-associated stromal cells (GASCs) from histologically normal surgical margins have a myofibroblast phenotype and angiogenic properties, J. Pathol. 233 (2014) 74–88.
[20] S. Jain, J.W. Rick, R.S. Joshi, A. Beniwal, J. Spatz, S. Gill, et al., Single-cell RNA sequencing and spatial transcriptomics reveal cancer-associated fibroblasts in glioblastoma with protumoral effects, J. Clin. Invest. 133 (2023) e147087.
[21] P.M. Galbo, A.T. Madsen, Y. Liu, M. Peng, Y. Wei, M.J. Ciesielski, et al., Functional contribution and clinical implication of cancer-associated fibroblasts in glioblastoma, Clin. Cancer Res. 30 (2024) 865–876.
[22] Y. Han, Y. Wang, X. Dong, D. Sun, Z. Liu, J. Yue, et al., TISCH2: expanded datasets and new tools for single-cell transcriptome analyses of the tumor microenvironment, Nucleic Acids Res. 51 (2023) D1425–D1431.
[23] T. Stuart, A. Butler, P. Hoffman, C. Hafemeister, E. Papalexi, W.M. Mauck, et al., Comprehensive integration of single-cell data, Cell 177 (2019) 1888–1902.e21.
[24] E. Becht, L. McInnes, J. Healy, C.-A. Dutertre, I.W.H. Kwok, L.G. Ng, et al., Dimensionality reduction for visualizing single-cell data using UMAP, Nat. Biotechnol. (2018).
[25] R. Moncada, D. Barkley, F. Wagner, M. Chiodin, J.C. Devlin, M. Baron, et al., Integrating microarray-based spatial transcriptomics and single-cell RNA-seq reveals tissue architecture in pancreatic ductal adenocarcinomas, Nat. Biotechnol. 38 (2020) 333–342.
[26] X. Qiu, Q. Mao, Y. Tang, L. Wang, R. Chawla, H.A. Pliner, et al., Reversed graph embedding resolves complex single-cell trajectories, Nat. Methods 14 (2017) 979–982.
[27] R.D. Bense, C. Sotiriou, M.J. Piccart-Gebhart, J.B.A.G. Haanen, M.A.T.M. van Vugt, E.G.E. de Vries, et al., Relevance of tumor-infiltrating immune cell composition and functionality for disease outcome in breast cancer, J. Natl. Cancer Inst. 109 (2017) djw192.
[28] E. Becht, N.A. Giraldo, L. Lacroix, B. Buttard, N. Elarouci, F. Petitprez, et al., Estimating the population abundance of tissue-infiltrating immune and stromal cell populations using gene expression, Genome Biol. 17 (2016) 218.
[29] K. Yoshihara, M. Shahmoradgoli, E. Martínez, R. Vegesna, H. Kim, W. Torres-Garcia, et al., Inferring tumour purity and stromal and immune cell admixture from expression data, Nat. Commun. 4 (2013) 2612.
[30] A. Mayakonda, D.-C. Lin, Y. Assenov, C. Plass, H.P. Koeffler, Maftools: efficient and comprehensive analysis of somatic variants in cancer, Genome Res. 28 (2018) 1747–1756.
[31] M.W. Beck, NeuralNetTools: visualization and analysis tools for neural networks, J. Stat. Software 85 (2018) 1–20.
[32] H. Wang, J. Yang, X. Li, H. Zhao, Current state of immune checkpoints therapy for glioblastoma, Heliyon 10 (2024) e24729.
[33] H. Munir, J.O. Jones, T. Janowitz, M. Hoffmann, M. Euler, C.P. Martins, et al., Stromal-driven and Amyloid β-dependent induction of neutrophil extracellular traps modulates tumor growth, Nat. Commun. 12 (2021) 683.
[34] X. Mao, J. Xu, W. Wang, C. Liang, J. Hua, J. Liu, et al., Crosstalk between cancer-associated fibroblasts and immune cells in the tumor microenvironment: new findings and future perspectives, Mol. Cancer 20 (2021) 131.
[35] K. Woroniecka, P. Chongsathidkiet, K. Rhodin, H. Kemeny, C. Dechant, S.H. Farber, et al., T-cell exhaustion signatures vary with tumor type and are severe in glioblastoma, Clin. Cancer Res. 24 (2018) 4175–4186.
[36] M.S. Alghamri, B.L. McClellan, R.P. Avvari, R. Thalla, S. Carney, C.S. Hartlage, et al., G-CSF secreted by mutant IDH1 glioma stem cells abolishes myeloid cell immunosuppression and enhances the efficacy of immunotherapy, Sci. Adv. 7 (2021) eabh3243.
[37] Y. Zhang, N. Lv, M. Li, M. Liu, C. Wu, Cancer-associated fibroblasts: tumor defenders in radiation therapy, Cell Death Dis. 14 (2023) 541.
[38] D.J. Kim, J.M. Dunleavey, L. Xiao, D.W. Ollila, M.A. Troester, C.A. Otey, et al., Suppression of TGFβ-mediated conversion of endothelial cells and fibroblasts into cancer associated (myo)fibroblasts via HDAC inhibition, Br. J. Cancer 118 (2018) 1359–1368.
[39] H. Xiang, H. Yu, Q. Zhou, Y. Wu, J. Ren, Z. Zhao, et al., Macrophages: a rising star in immunotherapy for chronic pancreatitis, Pharmacol. Res. 185 (2022) 106508.
[40] F. Wu, J. Yang, J. Liu, Y. Wang, J. Mu, Q. Zeng, et al., Signaling pathways in cancer-associated fibroblasts and targeted therapy for cancer, Signal Transduct. Targeted Ther. 6 (2021) 218.
[41] X. Chen, E. Song, Turning foes to friends: targeting cancer-associated fibroblasts, Nat. Rev. Drug Discov. 18 (2019) 99–115.
[42] S. Moatassim-Billah, C. Duluc, R. Samain, C. Jean, A. Perraud, E. Decaup, et al., Anti-metastatic potential of somatostatin analog SOM230: indirect pharmacological targeting of pancreatic cancer-associated fibroblasts, Oncotarget 7 (2016) 41584–41598.
[43] A.M. Santos, J. Jung, N. Aziz, J.L. Kissil, E. Puré, Targeting fibroblast activation protein inhibits tumor stromagenesis and growth in mice, J. Clin. Invest. 119 (2009) 3613–3625.
[44] M. Loeffler, J.A. Krüger, A.G. Niethammer, R.A. Reisfeld, Targeting tumor-associated fibroblasts improves cancer chemotherapy by increasing intratumoral drug uptake, J. Clin. Invest. 116 (2006) 1955–1962.